Sensors & Transducers, Vol. 246, Issue 7, November 2020, pp. 71-78

www.sensorsportal.com

Sensors & Transducers

Published by IFSA Publishing, S. L., 2020
http://www.sensorsportal.com

Graphene-Tin Oxide Composite Nanofibers for Low Temperature Detection of NO_2 and O_3

[1, *] Sergio MASA, [2] Diego ROBÉS, [1] Esther HONTAÑÓN, [3] Jesús LOZANO, [4] Siamak EQTESADI and [2] Adolfo NARROS

[1] Spanish National Research Council, Dept. of Sensors and Ultrasonic Systems, C/Serrano 144, Madrid, 28006, Spain
[2] Polytechnic University of Madrid, Dept. of Chemical Industrial and Environmental Engineering, C/José Gutiérrez Abascal 2, Madrid, 28006, Spain
[3] University of Extremadura, Dept. of Electrical, Electronic and Automation Engineering, Av. de Elvas s/n, Badajoz, 06006, Spain
[4] Abalonyx AS, Forskningsveien 1, 0373, Oslo, Norway
[*] E-mail: sergio.masa@csic.es

Received: 28 September 2020 /Accepted: 9 November 2020 /Published: 30 November 2020

Abstract: In this work we investigate the detection performance of nanofibers of tin oxide (SnO_2) towards sub-0.1 ppm nitrogen oxide (NO_2) and ozone (O_3) in air. It is found that SnO_2 nanofibers are more sensitive to O_3 than to NO_2, and the optimal working temperature differs significantly between the two gases: 200 ºC (NO_2) and 350 ºC (O_3). SnO_2 nanofibers loaded with reduced graphene oxide (rGO) show higher sensitivity than nanofibers of pure SnO_2 at low temperatures and the optimal working temperature diminishes by around 150 ºC for the two gases. The air humidity does not modify the optimum working temperature of rGO-loaded SnO_2 nanofibers but it affects their sensitivity at temperatures below 150 ºC. Irradiation with UV light is a promising method to activate gas desorption from rGO-loaded SnO_2 nanofibers so that this material could be used in chemiresistive sensors for low temperature detection of air pollutants.

Keywords: Tin oxide nanofibers, Reduced graphene oxide, Electrospinning, UV irradiation, Air pollution.

1. Introduction

Modern gas sensors are based on microelectromechanical system (MEMS) substrates coated with thick or thin films of metal oxide semiconductors (MOS) as sensitive material, which can be continuously heated to the optimal working temperature (<300 ºC) using a few tens of milliwatts. The power consumption and fabrication cost of MOS gas sensors need to be further reduced to enable their massive deployment in wireless sensor networks, and also sensing properties such as selectivity and sensitivity must be improved in the sub-0.1 ppm range for applications such as air pollution monitoring [1, 2].

Over the last decade, MOS nanostructures [3-6], especially one-dimensional (1D) nanostructures have being investigated for gas sensing because they large surface-to-volume ratio, high specific surface area, nano-size effects, superior stability, and ease of fabrication and functionalization [7-9]. Among 1D nanostructures, nanofibers have been identified as the most promising structures for use in gas sensors. They have higher surface-to-volume ratio than other 1D nanostructures due to the presence of a large number of nanograins and a web like configuration. Therefore,

their surfaces are readily exposed to gas molecules, resulting in high sensitivity and rapid response [10]. Although there are other techniques for the synthesis of nanofibers, most of MOS nanofibers for gas sensing applications are synthesized by the electrospinning method [11-13]. Nanostructured MOS layers prepared by electrospinning of polymer solutions containing metal precursors and subsequently calcined at high temperatures display unique fibrous morphologies. The combination of small grain size, high surface area, and high porosity that includes both small and large pores is ideally suited for gas sensing. From a commercial point of view, electrospinning is the only method of choice for the large scale preparation of nanofibers compared to other available methods, due to the easy handling, minimum consumption of solution, controllable nanofiber diameter, low cost, simple, and reproducibility in processing nanofibers [14, 15]. In addition, more recently, nanoscale MOS heterojunctions have received increasing attention as the most promising candidates to exhibit outstanding gas sensing performance, which is attributed to the adjustable highness of the potential barriers [16-18]. It has been found, for example, that the optimal working temperature of gas sensors using MOS/graphene heterojunctions is lower than that of MOS sensors, and eventually may be operated at room temperature [19, 20]. These results pave the way towards the industrial production of nanostructured MOS sensors by using affordable substrates such as polymers, and simple and easy to scale-up techniques like electrospinning.

Tin oxide (SnO_2) is the most well-known oxide and the most commonly used MOS in commercially available gas sensors for a wide variety of applications [21-25]. In this work, we assess the feasibility of electrospun SnO_2 nanofibers as sensing material in chemiresistive sensors for detecting air pollutants. In particular, the detection performance of SnO_2 nanofibers towards low level (<100 ppb) nitrogen dioxide (NO_2) and ozone (O_3) in air is studied as a function of the sensor operating temperature and air humidity. In addition, the effect of adding graphene to SnO_2 nanofibers and UV light irradiation are investigated in terms of the low temperature sensing behavior of SnO_2 nanofibers. The work shows promising results regarding the suitability of sensors based on nanofibers composed of SnO_2 and rGO for selective detection of NO_2 and O_3 at low temperature.

2. Experimental

2.1. Synthesis of Nanofibers

Nanofibers of SnO_2 were synthesized by electrospinning of an aqueous solution of polyvinyl-alcohol (PVA) and tin tetrachloride pentahydrate ($SnCl_4 \cdot 5H_2O$) followed by calcination of electrospun fibers, which results in solvent evaporation, polymer decomposition and tin oxidation [26]. The viscosity and the conductivity of the solution, and the process parameters were optimized as to control instability growth during electrospinning, which affects the morphology and structure of the nanofibers of SnO_2 [27, 28]. The composition and the method for the preparation of the solution, and the parameters for electrospinning are summarized in Tables 1 and 2, respectively. In addition, nanofibers of SnO_2 doped with graphene were prepared by adding a suspension of reduced graphene oxide (rGO, Abalonyx AS, Norway) in isopropanol (0.1 $mg \cdot ml^{-1}$) to the precursor solution and sonicating for half an hour. The content of rGO in the solution was 0.1 %wt with respect to Sn.

Samples of electrospun fibers of PVA loaded with tin were collected onto silicon (Si) substrates and calcined in ambient air at 500 ºC overnight. The X-ray diffractogram (XRD) of the as-prepared nanofibers is displayed in Fig. 1 (Malvern Panalytical Empyrean Cu LFF). The nanofibers exhibit pure SnO_2 rutile structure (JCPDS file no. 41-1445) with (110) and (101) as preferential crystalline orientations.

Table 1. Preparation of precursor solution.

Compound	%wt	Solution	Preparation
DI H_2O Quimipur 231-791-2	80	#1 DI H_2O PVA	magnetic stirring (50 rpm) & heating (90 ºC) 30 min
PVA Aldrich Chem. 341584	10	#2 DI H_2O $SnCl_4 \cdot 5H_2O$	magnetic stirring (50 rpm) 10 min
$SnCl_4 \cdot 5H_2O$ Sigma Aldrich 244678	10	#1 + #2 DI H_2O PVA $SnCl_4 \cdot 5H_2O$	mixing & magnetic stirring (50 rpm) overnight

Table 2. Electrospinning parameters.

Needle diameter (m)	Flowrate ($m^3 \cdot s^{-1}$)	Voltage (V)	Distance (m)
5×10^{-4}	3.3×10^{-8}	19×10^{3}	6×10^{-3}

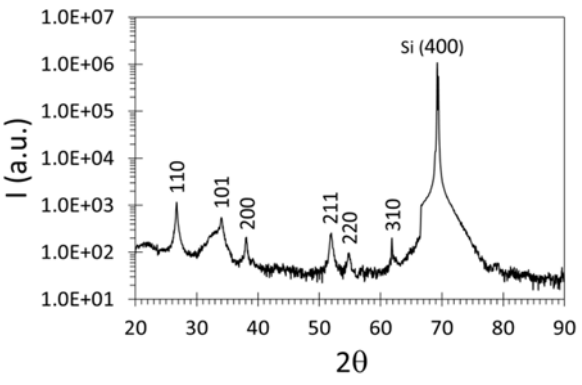


Fig. 1. XRD pattern of SnO_2 nanofibers on Si substrate.

Besides, the structure and the morphology of the SnO_2 nanofibers were analyzed by SEM, as displayed in Fig. 2 (Hitachi S-4800, 0.5-30 kV).

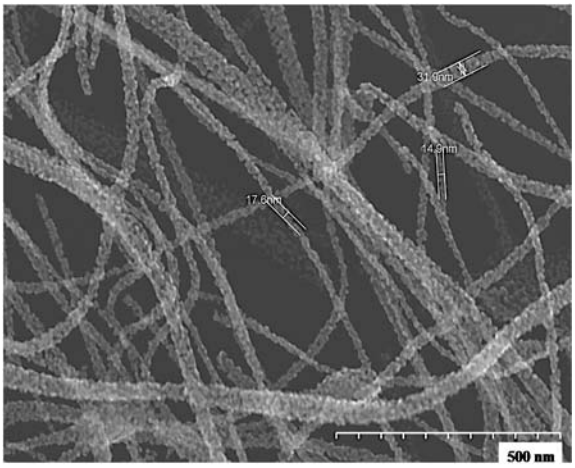


Fig. 2. SEM micrograph of electrospun SnO_2 nanofibers.

The nanofibers form a highly porous three-dimensional mat network on the substrate. The diameter of the nanofibers varies between 10 and 50 nm and it is rather uniform along the entire length of the nanofibers, of the order of tens of micrometers. The formation of SnO_2 nanofibers by calcination of electrospun Sn-loaded polymer fibers has been described by other authors [29, 30]. In all cases, SnO_2 nanofibers showed a hollow core-shell tubular structure with a granular shell consisting of SnO_2 grains of a few nanometers in size, which can be observed in Fig. 2 as well.

2.2. Preparation of Sensors

Sensors were prepared by depositing electrospun PVA fibers loaded with either Sn or Sn and rGO from the gas phase on a square silicon platform (side~4 mm) that is bonded to the surface of a circular TO8 header (diameter~15 mm). A picture of the multisensor silicon platform including four microhotplates is shown in Fig. 3. A microhotplate consists of a dielectric membrane (SiO_2/SiN_x) and two metallizations (Ti/Pt), interdigitated electrodes (IDTs) and a resistor or heater, practiced on the surface of a silicon substrate. The design and the manufacturing process of the microhotplate, and the calibration curve (I-V) of the microheater have been reported elsewhere [31].

Tin loaded PVA fibers were produced by electrospinning in ambient air at room temperature. The process maintained stable during at least 10 minutes, when the fibers deposited onto the surface of the TO8 header. Afterwards, the fibrous layer covering the IDTs (area~0.2 mm^2) was calcined by heating the layer with the help of the resistor lying underneath.

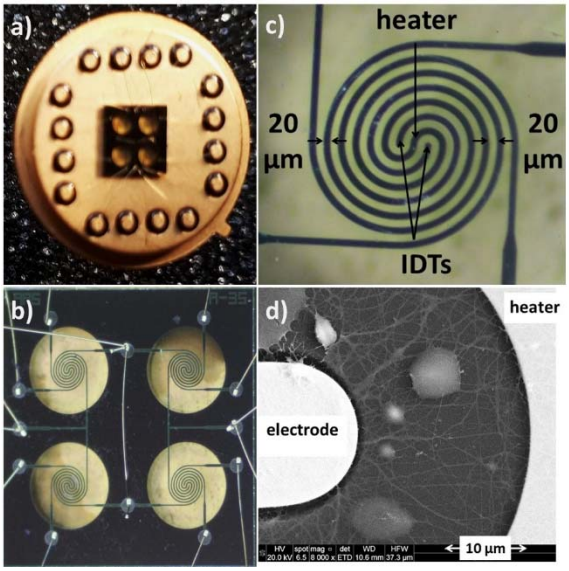


Fig. 3. a) Camera picture of TO8 header with multisensor platform on the top; Optical microscopy images of b) multisensor platform, and c) microhoplate; d) SEM micrograph of electrospun SnO_2 nanofibers onto microhotplate.

2.3. Characterization of Sensors for Gas Detection

We characterized the detection performance of the sensors based on nanofibers of SnO_2 and on nanofibers of SnO_2 loaded with rGO (hereinafter SnO_2:rGO) towards two air pollutants: NO_2 and O_3. For that purpose, we used calibration cylinders of gas mixtures of NO_2 in dry air, and generated mixtures of O_3 in dry air by using a commercial ozone generator based on a UV lamp and an air cylinder. In a gas mixing unit, the mixture NO_2-air from the cylinder or the mixture O_3-air from the ozone generator were diluted with air from a cylinder to attain the desired concentration of the gas in the mixture. Optionally, moisture can be added to the gas by flowing the gas stream throuhg a bubbler and, then, the gas entered the sensor cell. The latter has a free volume of 0.58 cm^3 and temperature and humidity sensors placed on its upper wall continuously monitored the ambient conditions inside the cell. The concentration of O_3 in the gas mixture was measured downstream of the sensor cell by using a commercial ozone monitor. The facility is completely automated and controlled from a program based on the LabView software [26].

In the experiments, the gas flowrate was set to 0.2 $l \cdot min^{-1}$, the concentration of NO_2/O_3 in the gas varied between 20 ppb and 200 ppb, and the air moisture ranged from 5 % to 80 % (relative humidity).

3. Results

3.1. Optimal Working Temperature

Sensors were exposed to mixtures NO_2-air and O_3-air followed by clean air and operated at

temperatures between 25 ºC and 350 ºC. SnO_2 behaved like an n-type semiconductor and its resistance increased in presence of the two oxidizing gases under study, in the range of sensor operating temperatures and gas concentrations covered in this work. As an example, Fig. 5 displays the evolution over time of the resistance of a sensor using nanofibers of SnO_2 in an experiment with a mixture of O_3 and dry air. A total of six adsorption-desorption cycles were completed for each sensor operating temperature.

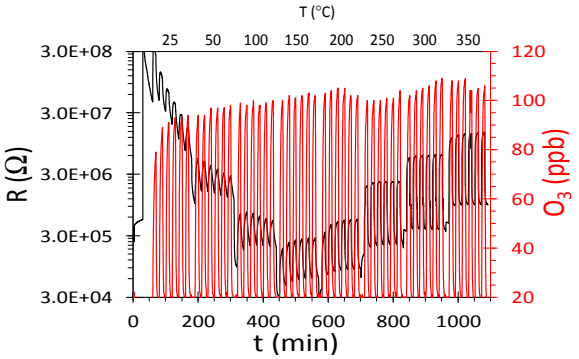


Fig. 5. Dynamic resistance curve of a sensor using electrospun SnO_2 nanofibers exposed to a mixture air-O_3 (~100 ppb) followed by clean dry air (≤5% RH) at different sensor operating temperatures (25-350 °C).

It is seen in Fig. 5 that the resistance of the sensor in clean dry air (gas desorption phase) has a parabolic profile with the sensor operating temperature and reaches a minimum at a temperature of around 150-200 °C. This result is consistent with measurements of the resistance of SnO_2 films published in the literature [32]. The increase in the sensor resistance for temperatures beyond 200°C is attributed to the interaction of oxygen with the surface of the SnO_2 nanofibers. Oxygen has a strong tendency to accept electrons from the metal oxide surface. Below 200 C, oxygen can accept one electron and above 200 °C, it can accept two electrons, with the consequent reduction in the electrical conductivity of the material [33]. Therefore, above 200 ºC atomic oxygen ions O^- form on the surface of SnO_2 nanograins, as follows

$$O_{2\,(ads)}^{-} + e^- \leftrightarrow 2O^-_{(ads)}, \quad (1)$$

$$O_{2(gas)} + 2e^- \leftrightarrow 2O^-_{(ads)} \quad (2)$$

Here the sensor response is defined as the ratio R_g/R_a; where R_a stands for the sensor resistance in air, before the start of the gas adsorption phase, and R_g is the resistance of the sensor when exposed to the target gas, at the end of the gas adsorption phase. The response of sensors based on nanofibers of SnO_2 and on nanofibers of SnO_2:rGO towards NO_2 and O_3 in dry air is plotted as a function of the sensor operating temperature in Fig. 6.

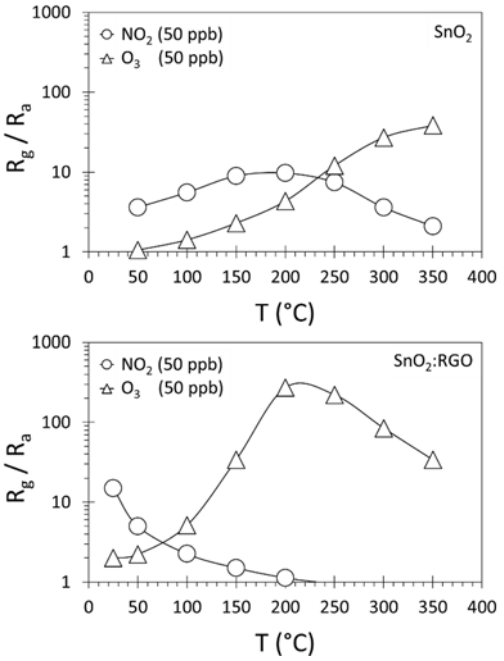


Fig. 6. Response of sensor using SnO_2 nanofibers and rGO-loaded SnO_2 nanofibers to NO_2 and O_3 in dry air (≤5 % RH) versus sensor working temperature.

It is seen in Fig. 6 that the optimal working temperature (i.e. the temperature at which the sensor response is maximum) of the sensors using SnO_2 nanofibers is of around 200 °C and 350 °C for NO_2 and O_3, respectively. These results are consistent with results obtained with sensors using SnO_2 thin films reported in the bibliography. As a rule, the maximum response of SnO_2 sensors is observed at temperatures below 250 ºC down to ambient temperature for NO_2 and above 250 ºC up to 500 ºC for O_3 [34, 35]. The kinetics of the interaction of NO_2 and O_3 with the SnO_2 lattice and with the chemisorbed oxygen ions on its surface has been described elsewhere [36, 37].

The response of SnO_2 nanofibers to NO_2 increases as the sensor operating temperature is raised from room temperature towards 200 °C. This result indicates that a thermally activated oxidation of SnO_2 surface is the dominant adsorption process in the low temperature range [38-40]. The predominant oxygen species on the SnO_2 surface is molecular oxygen ion O_2^-. With NO2 molecules being unlikely to react with O_2^- ions, a direct interaction with surface tin ions is likely

$$NO_{2(gas)} + e^- \leftrightarrow NO_{2\,(ads)}^{-} \quad (3)$$

As the sensor operating temperature is further raised, the availability of atomic oxygen ions O^- on the SnO2 surface increases drastically, as a result of reactions (1) and (2). In such a situation direct ionosorption reaction (3) becomes improbable. With significant amounts of O^- ions now being available on the surface, reactions such as

$$NO_{2(gas)} + O^-_{(ads)} \leftrightarrow NO_{(gas)} + O_{2(gas)} + e^- \quad (4)$$

become possible [38-40]. This is a reducing interaction that leads to a decrease in sensor resistance and also consumes NO_2. Then, in the high temperature range the sensor response is the result of the competition between reactions (3) and (4).

Ozone is a highly unstable and reactive gas that readily donates its extra oxygen atom, even at low temperatures. The following oxidizing reactions can occur at the SnO_2 surface under exposure to O_3

$$O_{3(gas)} + e^- \leftrightarrow O_{3\,(ads)}^-, \quad (5)$$

$$O_{3(gas)} + e^- \leftrightarrow O^-_{(ads)} + O_{2(gas)} \quad (6)$$

however, by analogy with oxygen, which has a larger dissociation energy than O_3, but already adsorbs dissociatively at the surface of SnO_2 above 150 ºC; it is believed that dissociative adsorption of O_3, reaction (6), is the preferred interaction above 100 ºC [37, 39]. In general, the maximum sensitivity to O_3 of sensors based on SnO_2 thin films has been observed in a temperature range when the SnO_2 surface is free from molecular water (>100 ºC) and the concentration of chemisorbed atomic oxygen ion O^- is still low. As the operating temperature of the sensor is raised, the concentration of O^- ions also increases and the following reaction initiates

$$O_{3(gas)} + O^-_{(ads)} \leftrightarrow 2O_{2(gas)} + e^- \quad (7)$$

a reducing interaction that results in a reduction of sensor response through the reduction of sensor resistance and the consumption of O_3 available for surface reactions.

As it can be seen in Fig. 6, by adding rGO to the SnO_2 nanofibers the sensor response in the low temperature range increases considerably and the optimal working temperature reduces by nearly 150 ºC, down to room temperature for NO_2 and 200 ºC for O_3. These results are attributed to the formation of local p-n heterojunctions between rGO flakes (p-type) and SnO_2 nanograins (n-type) on the inner and outer surface of the hollow SnO_2 nanofibers. A noticeable improvement of sensing performance towards NO_2 and other air pollutants has been found for SnO_2-graphene composite materials by other authors too [19, 41-46]. To the best of our knowledge, this is the first time that such behavior is reported for O_3.

Then, the effect of air humidity on sensor response was assessed. Fig. 7 compares the response of sensors using nanofibers of SnO_2:rGO towards NO_2 and O_3 in dry air and in humid air.

It can be seen that the optimal working temperature is not affected by air humidity, but it does affect the sensitivity of the sensor at low temperatures. Below 150 °C the sensor response towards NO_2 decreases as air humidity increases and the opposite occurs for O_3.

The effect of water vapor on the gas detection behavior of SnO_2 thin films has been widely investigated [47-49]. SnO_2 tends to absorb multiple layers of humidity from ambient air, forming a liquid water film on the surface. The active sensing layer in this case is the adsorbed water film, which responds only to gases that can easily dissolve and undergo electrolytic dissociation in water [50, 51]. Raising the substrate temperature towards 150 ºC, the water coverage drops and large patches of free SnO_2 surface appear, providing adsorption sites for water vapor and other gases in the air (O_2, NO_2, O_3).

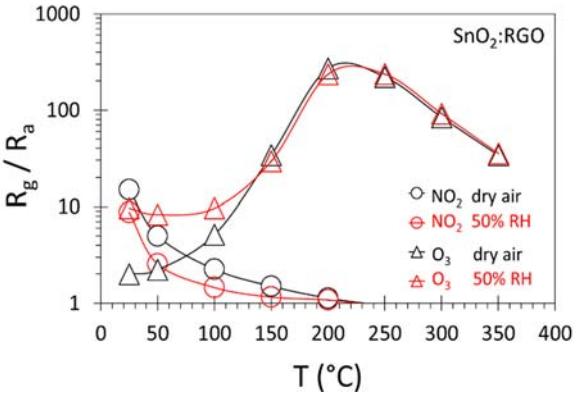


Fig. 7. Response of s sensor using RGO-loaded SnO_2 nanofibers to NO_2 and O_3 in dry air and in humid air (50 % RH) versus working temperature. The concentration of the gases is 50 ppb.

3.2. Recovery Speed

The results suggest using electrospun nanofibers of SnO_2:rGO as sensing material for selective detection of NO_2 and O_3 in air. Acceptable operating temperatures are below 100 ºC for NO_2 and between 100 ºC and 200 ºC for O_3. However, the slow recovery of MOS sensors at such low temperatures limits its suitability to air pollution monitoring.

Fig. 8 shows the recovery behavior of a sensor using SnO_2:rGO nanofibers after exposure to O_3 in humid air at various working temperatures. The recovery time τ_{rec} is the time it takes for the change in the sensor response when exposed to the gas to be reduced by 90 % once the gas is removed. The recovery time is depicted as a function of the sensor operating temperature in Fig. 8 (inset).

The recovery time decreases with increasing temperature and reaches values acceptable for practical applications (τ_{rec}<30 s) at around 200 ºC. Therefore, the sensors should be operated in dynamic (variable temperature) mode instead of isothermal (constant temperature) mode, i.e. at low temperature for gas adsorption and high temperature for gas desorption [52, 53].

Also, it has been demonstrated that the low temperature sensing performance of MOS sensors can be improved by irradiation with UV light [54-59]. Here we investigate UV irradiation for low temperature gas desorption from RGO-loaded SnO_2 nanofibers. To that aim, we use a UV-LED source with peak wavelength λ_{max} at 356 nm (OSA Opto Light, OCU-400 UB355). The UV lamp is placed centered on the top wall of the sensor cell facing the surface of

the multisensor platform at a distance of nearly one cm. Sensors are subjected to adsorption-desorption cycles in which the sensor temperature is kept constant and the UV lamp is switched on only in the gas desorption phase.

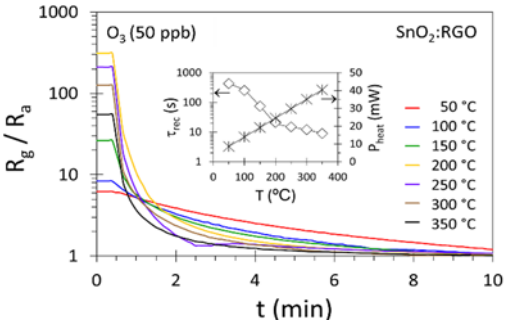


Fig. 8. Recovery behavior of a sensor using RGO-loaded SnO_2 nanofibers after exposure to O_3 (50 ppb) in humid air (50 % RH) at different working temperatures. Insert: Sensor recovery time (diamonds) and sensor heating power (crosses) versus working temperature.

Fig. 9 shows the response and the recovery time of a sensor in a test with a mixture of O_3 and humid air, the sensor operating and 100 °C, and the power of the UV source varying from null (lamp off) up to 55 mW. It can be observed that UV irradiation causes an enhancement of the sensor response and a reduction of the sensor recovery time, even at the lowest power of 3.3 mW used in the tests. A kind of saturation stage is reached at around 20 mW with a recovery time in the order of 60 s.

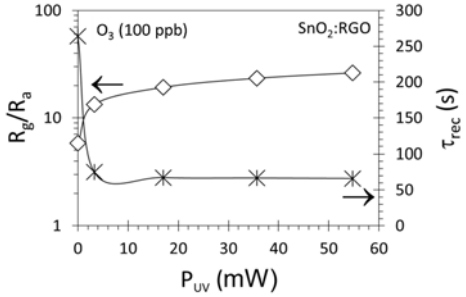


Fig. 9. Response (diamonds) / recovery time (crosses) of a sensor using RGO-loaded SnO_2 nanofibers under / after exposure to O_3 (100 ppb) in humid air (40 % RH) versus power of UV lamp in the desorption phase. The sensor operates in isothermal mode at 100 ºC.

Finally, we assess the stability of the sensors working in

1) Dynamic mode: 100 ºC for gas detection (T_{ads}) and 200 °C for sensor recovery (T_{des}), no UV irradiation;

2) Dynamic mode: 100 °C for gas detection and 350 °C for sensor recovery (T_{des}), no UV irradiation;

3) Isothermal mode: 100 °C for gas detection and sensor recovery, UV irradiation at 5 mA for gas desorption.

The tests run for 16 h and consist of 50 cycles, each of a duration of 20 min: 10 min for gas adsorption (T_{ads}), 5 min for sensor heating ($T_{ads} \rightarrow T_{des}$) and gas desorption ($T_{des}$), and 5 min for sensor cooling ($T_{des} \rightarrow T_{ads}$). In 3) both T_{ads} and T_{des} are set to 100 °C. The evolution of the sensor response in tests with O_3 in humid air is displayed in Fig. 10.

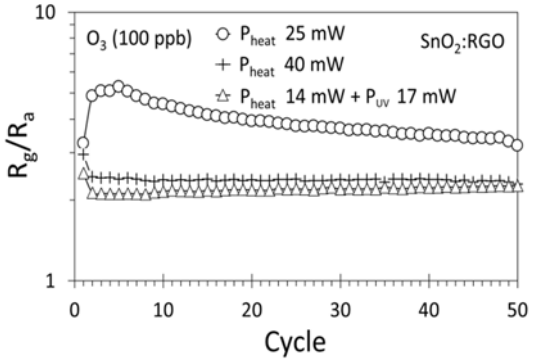


Fig. 10. Response of a sensor using RGO-loaded SnO_2 nanofibers under exposure to O_3 (100 ppb) in humid air (40 % RH) over adsorption-desorption cycles. Sensor temperature for gas adsorption is 100 °C and for gas desorption: 200 °C (P_{heat} 25 mW), 350 °C (P_{heat} 40 mW), and 100 ºC (P_{heat} 14 mW) with UV irradiation at 5 mA (P_{UV} 17 mW).

The sensor shows a rather similar response, both in value and stability, in tests 2) and 3). However, the power consumption of the sensor in the gas desorption phase is lower in test 3). Assuming that UV irradiation affects the four sensors equally, each sensor consumes around 18.25 mW for gas desorption in test 3), compared to 40 mW in test 2).

4. Conclusions

It has been demonstrated the feasibility of electrospun SnO_2:rGO nanofibers for selective detection of NO_2 and O_3 in air at temperatures below 100 °C with good sensitivity in the sub-0.1 ppm range. It has also been proven that thermal activation and UV photoactivation can effectively speed-up gas desorption from the nanofibers of SnO_2:rGO at low temperatures. For practical applications it is still necessary to design and assess heating and UV irradiation strategies that guarantee the stability of the sensor in the long-term.

Acknowledgements

The Interreg-Sudoe Programme of the European Union (EU) is acknowledged for funding this research (Grant Agreement SEO2/P1/E569, NanoSen-AQM, www.nanosenaqm.eu).

References

[1]. Ph. J. D. Peterson, A. Aujla, K. H. Grant, A. G. Brundle, M. R. Thompson, J. V. Hey, R. J. Leigh, Practical use of metal oxide semiconductor gas sensors for measuring nitrogen dioxide and ozone in urban environments, *Sensors*, Vol. 17, Issue 7, 2017, 1653 (25 pp).

[2]. D. G. Rickerby, A. N. Skouloudis, Application of nanocrystalline metal oxide gas sensors for air quality monitoring, *International Journal of Nanotechnology* Vol. 11, Issue 5/6/7/8, 2014, pp. 583-593.

[3]. D. Nunes, A. Pimentel, A. Goncalves, S. Pereira, R. Branquinho, P. Barquinha, E. Fortunato, R. Martins, Metal oxide nanostructures for sensor applications, *Semiconductor Science and Technology*, Vol. 34, Issue 4, 2019, 043001 (178 pp).

[4]. F. Sarf, Metal oxide gas sensors by nanostructures, *IntechOpen*, 2019, 88858 (18 pp).

[5]. G. Korotcenkov, Metal oxide-based nanostructures, in Handbook of Gas Sensor Materials, Integrated Analytical Systems, *Springer*, 2014, Chapter 3, pp. 47-67.

[6]. N. A. Shah, M. Gul, M. Abbas, M. Amin, Synthesis of metal oxide semiconductor nanostructured for gas sensors, *IntechOpen*, 2019, 86815 (24 pp).

[7]. G. Korotcenkov, Current trends in nanomaterials for metal-oxide conductometric gas sensors: Advantages and limitations, Part 1: 1D and 2D nanostructures, *Nanomaterials*, Vol. 10, 2020, 1392 (62 pp).

[8]. N. Kaur, M. Singh, E. Comini, One-dimensional nanostructured oxide chemoresistive sensors, *Langmuir*, Vol. 36, 2020, pp. 6326-6344.

[9]. M. M. Arafat, B. Dinan, S. A. Akbar, A. S. M. A. Haseeb, Gas sensors based on one dimensional nanostructured metal-oxides: A review, *Sensors*, Vol. 12, Issue 6, 2012, pp. 7207-7258.

[10]. A. Katoch, Gas sensor: 1D semiconductor metal oxide nanomaterials: Interface engineering of metal oxide nanofibers, *Lap Lambert Academic Publishing*, 2016, pp. 1-308.

[11]. M. Imran, N. Motta, M. Shafiei, Electrospun one-dimensional nanostructures. A new horizon for gas sensing materials, *Beilstein Journal of Nanotechnology*, Vol. 9, 2018, pp. 2128-2170.

[12]. Z. U. Abideen, J.-H. Kim, J.-H. Lee, J.-Y. Kim, A. Mirzaei, H. W. Kim, S. S. Kim, Electrospun metal oxide composite nanofibers gas sensors – A review, *Journal of the Korean Ceramic Society*, Vol. 54, Issue 5, 2017, pp. 366-379.

[13]. L.-D. Kim, A. Rothschild, Nanostructured metal oxide gas sensors prepared by electrospinning, *Polymers for Advanced Technologies*, Vol. 22, Issue 3, 2011, pp. 318-325.

[14]. A. M. Al-Dhahebi, S. Ch. B. Gopinath, M. S. M. Saheed, Graphene impregnated electrospun nanofiber sensing materials: A comprehensive overview on bridging laboratory set-up to industry, *Nano Convergence*, Vol. 7, Issue 1, 2020, 27, (23 pp.).

[15]. L. Persano, A. Camposeo, C. Tekmen, D. Pisignano, Industrial upscaling of electrospinning and applications of polymer nanofibers: A review, *Macromolecular Materials and Engineering*, Vol. 298, Issue 5, 2013, pp. 504-520.

[16]. S. Yang, Z. Wang, G. Lei, H. Xu, Y. Hu, H. Gu, High-performance gas sensors based on nanostructured metal oxide heterojunctions, in Functional Nanomaterials, Materials Horizons: From Nature to Nanomaterials, S. Thomas, N. Johsi, V. Tomer, *Springer*, 2020, pp. 19-70.

[17]. D. Zappa, V. Galstyan, N. Kaur, H. M. M. M. Arachchige, O. Sisman, E. Comini, Metal oxide-based heterostructures for gas sensors: A review, *Analytical Chimica Acta*, Vol. 1039, 2018, pp. 1-23.

[18]. D. R. Miller, S. A. Akbar, P. A. Morris, Nanoscale metal oxide-based heterojunctions: A review, *Sensors and Actuators B*, Vol. 204, 2014, pp. 250-272.

[19]. D. Sun, Y. Luo, M. Debliquy, Ch. Zhang, Graphene-enhanced metal oxide gas sensors at room-temperature. A review, *Beilstein Journal of Nanotechnology*, Vol. 9, Issue 1, 2018, pp. 2832-2844.

[20]. M. M. Hossain, Metal oxide semiconductor/graphene heterojunctions based sensors, *All Theses*, Clemson University, South Caroline, USA, 2017, 2754, (137 pp.).

[21]. A. Staerz, T. Suzuki, U. Weimar, N. Barsan, SnO_2: The most important base material for semiconducting metal oxide-based materials, in Tin Oxide Materials: Synthesis, Properties, and Applications, Ed. M. O. Orlandi, *Elsevier*, 2020, Chapter 12, pp. 346-377.

[22]. K. Aguir, S. Bernardini, B. Lawson, T. Fiorido, Trends in metal oxide thin films: Synthesis and applications of tin oxide, in Tin Oxide Materials: Synthesis, Properties, and Applications, Ed. M. O. Orlandi, *Elsevier*, 2020, Chapter 8, pp. 219-246.

[23]. G. Velmathi, S. Mohan, R. Henry, Analysis and review of tin oxide chemoresistive gas sensors, *IETE Technical Review*, Vol. 33, Issue 3, 2015, pp. 323-331.

[24]. B. Yuliarto, G. Gumilar, N. L. W. Septiani, SnO_2 nanostructure as pollutant gas sensors: Synthesis, sensing performances, and mechanisms, *Advances in Materials Science and Engineering*, Vol. 2015, 694823, (14 pp.).

[25]. S. Das, V. Jayaraman, SnO_2: A comprehensive review on structures and gas sensors, *Progress in Materials Science*, Vol. 66, 2014, pp. 112-255.

[26]. S. Masa, D. Robés, E. Hontañón, J. Lozano, S. Eqtesadi, A. Narros, Graphene-loaded tin oxide nanofibers for low temperature detection of air pollutants, in *Proceedings of the 6th International Conference on Sensors Engineering and Electronics Instrumentation Advances (SEIA'2020)*, Porto, Portugal, 23-25 September 2020, pp. 27-32.

[27]. S. Bagchi, R. Brar, B. Singh, C. Ghanshyam, Instability controlled synthesis of tin oxide nanofibers and their gas sensing properties, *Journal of Electrostatics*, Vol. 78, 2015, pp. 68-78.

[28]. K. Garg, G. L. Bowlin, Electrospinnig jets and nanofibrous structures, *Biomicrofluidics*, Vol. 5, Issue 1, 2011, 013403, (19 pp.).

[29]. X. Zhang, G. Xu, H. Wang, H. Cui, X. Zhan, L. Sang, G. Zhang, Preparation of meso-porous SnO_2 fibers with enhanced sensitivity for n-butanol, *Ceramics International*, Vol. 44, 2018, pp. 4990-4995.

[30]. X. Xia, X. J. Dong, O. F. Wei, Y. B. Cai, K. Y. Lu, Formation mechanism of porous hollow SnO_2 nanofibers prepared by one-step electrospinning, *eXPRESS Polymer Letters*, Vol. 6, Issue 2, 2012, pp. 169-176.

[31]. P. Yoboué, A. Konaté, O. Asseu, Ph. Menini, An industrializable silicon-based microhotplate for metal oxides gas sensors, *Physical and Chemical News*, Vol. 72, 2014, pp. 34-41.

[32]. K. Nomura, H. Shiozawa, T. Takada, H. Reuther, E. Ritcher, Gas-sensor properties of SnO_2 films implanted with gold and iron ions, *Journal of*

Materials Science: Materials in Electronics, Vol. 8, Issue 5, 1997, pp. 301-306.

[33]. P. Shankar, J. B. B. Rayappan, Gas sensing mechanism of metal oxides: The role of ambient atmosphere, type of semiconductor and gases – A review, *Science Letters Journal*, Vol. 4, 2015, 126, (18 pp.).

[34]. G. Korotcenkov, V. Brinzari, B. K. Cho, In_2O_3- and SnO_2-based ozone sensors: Design and characterization, *Critical Reviews in Solid State and Materials Sciences*, Vol. 43, Issue 2, 2018, pp. 83-132.

[35]. A. Sharma, M. Tomar, V. Gupta, SnO_2 thin film sensor with enhanced response for NO_2 gas at lower temperatures, *Sensors and Actuators B*, Vol. 156, Issue 2, 2011, pp. 743-752.

[36]. A. V. Marikutsa, M. N. Rumyantseva, A. M. Gaskov, A. M. Samoylov, Nanocrystalline tin dioxide: Basics in relation with gas sensing phenomena Part II. Active centers and sensor behavior, *Inorganic Materi*als, Vol. 52, Issue 13, 2016, pp. 1311-1338.

[37]. G. Korotcenkov, V. Brinzari, B. K. Cho, In_2O_3- and SnO_2-based thin film ozone sensors: Fundamentals, *Journal of Sensors*, Vol. 2016, 3816094, pp. 1-31.

[38]. H. Liu, J. Wan, Q. Fu, M. Li, W. Luo, Z. Zheng, H. Cao, Y. Hu, D. Zhou, Tin oxide films for nitrogen dioxide gas detection at low temperatures, *Sensors and Actuators B*, Vol. 177, 2013, pp. 460-466.

[39]. L. Berry, J. Brunet, Oxygen influence on the interaction mechanisms of ozone on SnO_2 sensors, *Sensors and Actuators B*, Vol. 129, Issue 1, 2008, pp. 450-458.

[40]. B. Ruhland, Th. Becker, G. Müller, Gas-kinetic interactions of nitrous oxides with SnO_2 surface, *Sensors and Actuators B*, Vol. 50, Issue 1, 1998, pp. 85-94.

[41]. Z. U. Abideen, J. Y. Park, H. W. Kim, S. S. Kim, Graphene-loaded tin oxide nanofibers: Optimization and sensing performance, *Nanotechnology*, Vol. 28, Issue 3, 2017, 035501.

[42]. J.-H. Lee, A. Katoch, S.-W. Choi, J.-H. Kim, H. W. Kim, S. S. Kim, Extraordinary improvement of gas-sensing performances in SnO_2 nanofibers due to the creation of local p-n heterojunctions by loading reduced graphene oxide nanosheets, *ACS Applied Materials & Interfaces*, Vol. 7, Issue 5, 2015, pp. 3101-3109.

[43]. R. Ghosh, A. K. Nayak, S. Santra, D. Pradhan, P. K. Guha, Enhanced ammonia sensing at room temperature with reduced graphene oxide/tin oxide hybrid films, *RSC Advances*, Vol. 5, Issue 62, 2015, pp. 50165-50173.

[44]. G. Neri, S. G. Leonardi, M. Latino, N. Donato, S. Baek, D. E. Conte, P. A. Russo, N. Pinna, Sensing behavior of SnO_2/reduced graphene oxide nanocomposites toward NO_2, *Sensors and Actuators B*, Vol. 179, 2013, pp. 61-68.

[45]. P. A. Russo, N. Donato, S. G. Leonardi, S. Baek, D. E. Conte, G. Neri, N. Pinna, Room-temperature hydrogen sensing with hetereonanostructures based on reduced graphene oxide and tin oxide, *Angewandete Chemie International Edition*, Vol. 51, Issue 44, 2012, pp. 11053-11057.

[46]. Q. Lin, Y. Li, M. Yang, Tin oxide/graphene composite fabricated via a hydrothermal method for gas sensors working at room temperature, *Sensors and Actuators B*, Vol. 173, 2012, pp. 139-147.

[47]. D. Degler, Spectroscopic insights in the gas detection mechanism of tin dioxide based gas sensors, *PhD Thesis*, Furtwangen University, Tübingen, Germany, 2017.

[48]. R. G. Pavelko, The influence of water vapor on the gas sensing phenomenon of tin dioxide-based gas sensors, in Tin Chemical Sensors: Simulation and Modeling, G. Korotcenkov, *Momentum Press*, 2012, Chapter 8, (42 pp.).

[49]. G. Korotcenkov, I. Blinov, V. Brinzari, J. R. Stetter, Effect of air humidity on gas response of SnO_2 thin film ozone sensors, *Sensors and Actuators B: Chemical*, Vol. 122, Issue 2, 2007, pp. 519-526.

[50]. K. Maier, A. Helwig, G. Müller, P. Hille, M. Eickhoff, Effect of water vapor and surface morphology on the low temperature response of metal oxide semiconductor gas sensors, *Materials*, Vol. 8, Issue 9, 2015, pp. 6570-6588.

[51]. A. Helwig, G. Müller, G. Sberveglieri, M. Eickhoff, On the low-temperature response of semiconductor gas sensors, *Journal of Sensors*, Vol. 2009, 620720, (17 pp.).

[52]. R. Boiger, S. Defregger, M. Grbic, A. Köck, M. Mücke, R. W. Teubenacher, B. Z. Travieso, Exploring temperature-modulated operation mode of metal oxide gas sensors for robust signal processing, *Proceedings*, Vol. 2, 2018, 1058, (5 pp.).

[53]. A. P. Lee, B. J. Reedy, Temperature modulation in semiconductor gas sensing, *Sensors and Actuators B: Chemical*, Vol. 60, Issue 1, 1999, pp. 35-42.

[54]. R. Kumar, X. Liu, J. Zhang, M. Kumar, Room-temperature gas sensors under photoactivation: From metal oxides to 2D materials, *Nano-Micro Letters*, Vol. 12, 2020, 164, (37 pp.).

[55]. W. Li, J. Guo, L. Cai, W. Qi, Y. Sun, J.-L. Xu, M. Sun, H. Zhu, L. Xiang, D. Xie, T. Ren, UV light irradiation enhanced gas sensor selectivity of NO_2 and SO_2 using rGO functionalized with hollow SnO_2 nanofibers, *Sensors and Actuators B*, Vol. 290, 2019, pp. 443-452.

[56]. E. Espid, F. Taghipour, UV-LED photo-activated chemical gas sensors: A review, *Critical Reviews in Solid State and Materials Sciences*, Vol. 42, Issue 5, 2017, pp. 416-432.

[57]. F. H. Saboor, T. Ueda, K. Kamada, T. Hyodo, Y. Mortazavi, A. A. Khodadadi, Y. Shimizu, Enhanced NO_2 gas sensing performance of bare and Pd-loaded SnO_2 thick film sensors under UV-light irradiation at room temperature, *Sensors and Actuators B*, Vol. 223, 2016, pp. 429-439.

[58]. J. D. Prades, R. Jiménez-Díaz, F. Hernández-Ramírez, S. Barth, A. Cirera, A. Romano-Rodríguez, S. Mathur, J. R. Morante, Equivalence between thermal and room temperature UV light-modulated responses of gas sensors based on individual SnO_2 nanowires, *Sensors and Actuators B*, Vol. 140, Issue 2, 2009, pp. 337-341.

[59]. E. Comini, G. Faglia, G. Sberveglieri, UV light activation of tin oxide thin film for NO_2 sensing at low temperatures, *Sensors and Actuators B*, Vol. 78, Issues 1-3, 2001, pp. 73-77.

Published by International Frequency Sensor Association (IFSA) Publishing, S. L., 2020 (http://www.sensorsportal.com).